



**Black Phosphorus Quantum Dots as Dual-Functional  
Electron Selective Materials for Efficient Plastic Perovskite  
Solar Cells**

Journal:	<i>Journal of Materials Chemistry A</i>
Manuscript ID	TA-COM-02-2018-001408.R1
Article Type:	Communication
Date Submitted by the Author:	10-Apr-2018
Complete List of Authors:	<p>Fu, Nianqing; South China University of Technology, School of Materials Science and Engineering  Huang, Chun; Shenzhen University  Lin, Peng; Shenzhen University, College of Materials Science and Engineering  Zhu, Mingshan; Jinan University, School of Environment; Osaka University, The Institute of Scientific and Industrial Research  Li, Tao; Shenzhen University  Ye, Mao; Shenzhen University  LIN, Shenghuang; The Hong Kong Polytechnic University  Zhang, Guoge; South China University of Technology, School of Materials Science  Du, Jun; South China University of Technology  Liu, Chang; Southern University of Science and Technology  Xu, Baomin; Southern University of Science and Technology, Department of Materials Science and Engineering  Wang, Danyang; The University of New South Wales, School of Materials Science and Engineering  Ke, Shanming; Shenzhen University, College of Materials Science and Engineering</p>

# Black Phosphorus Quantum Dots as Dual-Functional Electron Selective Materials for Efficient Plastic Perovskite Solar Cells

Nianqing Fu,<sup>a\*</sup> Chun Huang,<sup>b</sup> Peng Lin,<sup>b</sup> Mingshan Zhu,<sup>c</sup> Tao Li,<sup>d</sup> Mao Ye,<sup>b</sup> Shenghuang Lin,<sup>d\*</sup> Guoge Zhang,<sup>a</sup> Jun Du,<sup>a</sup> Chang Liu,<sup>e</sup> Baomin Xu,<sup>e</sup> Danyang Wang,<sup>f</sup> and Shanming Ke,<sup>b, g\*</sup>

<sup>a</sup> School of Materials Science and Engineering, South China University of Technology, Guangzhou 510640, P. R. China.

*E-mail:* [msnqfu@scut.edu.cn](mailto:msnqfu@scut.edu.cn)

<sup>b</sup> Guangdong Research Center for Interfacial Engineering of Functional Materials, College of Materials Science and Engineering, Shenzhen University, Shenzhen 518060, P. R. China.

*E-mail:* [smke@szu.edu.cn](mailto:smke@szu.edu.cn)

<sup>c</sup> School of Environment, Jinan University, Guangzhou 510632, P. R. China

<sup>d</sup> Department of Applied Physics, The Hong Kong Polytechnic University, Hong Kong, P. R. China.

*E-mail:* [shenghuanglinchina@gmail.com](mailto:shenghuanglinchina@gmail.com)

<sup>e</sup> Department of Materials Science and Engineering, Southern University of Science and Technology, Shenzhen 518055, P. R. China.

<sup>f</sup> School of Materials Science and Engineering, The University of New South Wales, Sydney, New South Wales 2052, Australia.

<sup>g</sup> School of Materials Science and Engineering, Nanchang University, Nanchang 330031, Jiangxi, P. R. China.

**Abstract**

Organic-inorganic hybrid metal halide perovskite solar cells (PSCs) have attracted tremendous research interests due to their high power conversion efficiency and simple fabrication. However, exploitations of new electron selective materials which can simultaneously tailor the quality of metal halide perovskite film for low-temperature produced plastic organic-inorganic halide perovskite solar cells (PSCs) are of the key importance but remain a great challenge. Herein, facile solution processed black phosphorus quantum dots (BPQDs) with ambipolar conductivity are developed as dual-functional electron selective layer (ESL) in plastic PSCs. The BPQDs ESL plays crucial roles in both forming cascade energy level for fast electron extraction and guiding crystallization behavior of the perovskite to yield compact perovskite films with less traps, good crystallization and ordered orientation. The perovskite films deposited on the BPQDs ESL exhibit excellent optoelectronic properties and the resulting plastic planar perovskite solar cells possess a reasonably high efficiency of 11.26%. The 3.15-fold enhancement in efficiency arises from both the efficient electron extraction and suppressed radiative and trap-assisted non-radiative recombination, compared with the devices built on the bare ITO surface without an ESL. This work paves a promising way for developing novel electron selective non-oxide materials for highly efficient solar cells.

**Keywords:** black phosphorus quantum dots; perovskite solar cell; flexible; low temperature; electron extraction

## 1. Introduction

Organic-inorganic halide perovskite solar cells (PSCs) have brought a revolution to photovoltaic technologies, as their power conversion efficiency have been arisen dramatically from 3.8% in 2009 to 22.1% in 2016.<sup>1,2</sup> Thus far, the TiO<sub>2</sub> was deemed as the most successful ESL at delivering high efficiency for PSCs.<sup>2-4</sup> However, the mobility of TiO<sub>2</sub> is at least two orders of magnitude lower than the other components, namely perovskite and hole transport layer, of PSCs,<sup>3,4</sup> which dominates the limitation for further improvement in efficiency. More importantly, TiO<sub>2</sub> would catalyze the decomposition of organic-inorganic perovskite under ultraviolet irradiation and lead to serious instability of the devices.<sup>5,6</sup> Usually, a high-quality TiO<sub>2</sub> ESL often requires sophisticated high-temperature treatment above 450°C or high vacuum process (*e.g.* sputtering, pulsed laser deposition),<sup>7</sup> which acts as barriers to low-cost and fast mass production of PSCs for commercialization. Moreover, the high-temperature process is excluded when the devices are designed on plastic substrate for flexible solar cells which have the merits of lightweight, flexibility, suitable for roll-to-roll manufacturing, and convenience of integration.<sup>7-9</sup> Recently, many efforts have been devoted to developing some substitutes, including fullerene and its derivatives,<sup>10,11</sup> organic molecules,<sup>12</sup> solid-state ionic liquid and a series of metal oxides/sulfide (*e.g.* Al<sub>2</sub>O<sub>3</sub>, ZnO, SnO<sub>2</sub>, WO<sub>x</sub>, Nb<sub>2</sub>O<sub>5</sub>, In<sub>2</sub>O<sub>3</sub>, Zn<sub>2</sub>SnO<sub>4</sub>, In<sub>2</sub>S<sub>3</sub>, *etc.*)<sup>13-22</sup> to replace TiO<sub>2</sub> as ESL for low-temperature processed rigid or flexible PSCs (See more detailed information in Table S1 in Supporting Information). Among them, fullerene and its derivatives perform excellent in PSCs. However, their are expensive and the designed device configuration usually has to be restricted to an inverted structure mainly because of the wettability nature of those materials. ZnO and SnO<sub>2</sub>, which can be simply prepared by a cost-effective solution-processing technique, are the most common choices of metal oxides employed as ESL for low-temperature produced PSCs with promising

performance. However, the thermal instability of ZnO is the most denounced drawback to affect the stability of PSCs. In this regard, it is still crucial and urgent to develop more potentially alternative ESL materials which can be obtained through a simple and low-temperature process, even some impressive successes have already achieved.

In the past few years, two dimensional (2D) materials, such as graphene and transition-metal dichalcogenides (TMDs), have evoked tremendous interests as a class of promising materials for nanodevices, owing to their intriguing physical properties.<sup>22-25</sup> However, devices based on these materials suffer from some major drawbacks, such as the lack of a bandgap in graphene and considerable low conductive of the TMDs.<sup>22,24,25</sup> As a new member of 2D material family, black phosphorus (BP), a rare allotrope of phosphorus, has recently attracted enormous attention due to its inherently fascinating features of high theoretical mobility, tunable direct bandgap, ambipolarity and simple fabrication.<sup>24,26-29</sup> The bandgap of BP can be tuned from 0.3 eV for bulk to near 2.0 eV for monolayer form.<sup>24,28,29</sup> Moreover, when the BP appears in the form of quantum dots, it exhibits more amazing and unique electronic and optical properties, owing to the quantum confinement and edge effects.<sup>25,29</sup> As an elemental semiconductor, BP shows an ambipolar conductivity for both electron and hole.<sup>24,28,29</sup> The electron and hole mobility can be up to  $\sim 220$  and  $350 \text{ cm}^2 \text{ V}^{-1} \text{ s}^{-1}$  at room temperature, respectively, for its polycrystalline form.<sup>30</sup> The electron mobility of BP is roughly three orders of magnitude higher than that of  $\text{TiO}_2$  ( $0.1\sim 4 \text{ cm}^2 \text{ V}^{-1} \text{ s}^{-1}$ ).<sup>31</sup> Very recently, both single- or few-layered phosphorene nanosheets and black phosphorus quantum dots (BPQDs) have been explored as promising materials for field-effect transistors,<sup>32</sup> photodetector,<sup>33</sup> photocatalysis,<sup>34,35</sup> photoelectronics,<sup>36</sup> supercapacitors,<sup>37</sup> lithium/sodium ion batteries,<sup>38</sup> and solar cells.<sup>39-42</sup> Guo and Yan et al. exploited BPQDs as light-harvesting enhancer for dye-sensitized solar cells and organic photovoltaics (OPVs), respectively, to increase the light

utilization.<sup>39,40</sup> He demonstrated that the BPQD can employ for interface modifications of hole transport layer to enhance the charge extraction of solar cells.<sup>41</sup> Lau's work suggested that the modification of ZnO electron transport layer by BP flakes can promote the electron extraction from the excited active film,<sup>42</sup> indicating the potential of BP as an electron selective materials. However, using BPQDs as ESL alone in solar cells, especially for the plastic ones, has never been reported.

In this work, we present that BPQDs, prepared by facile liquid-exfoliation, show an ambipolar conductivity and were successfully exploited as dual-functional ESL for low-temperature processed plastic PSCs. The crafted BPQDs can offer suitable energy bands to form a desired band alignment, which facilitates electron extraction but rejects hole injection from the FA<sub>0.85</sub>MA<sub>0.15</sub>PbI<sub>2.5</sub>Br<sub>0.5</sub> perovskite to the ESL. Meanwhile, the BPQDs can facilitate the formation of dense perovskite film with good crystallization and ordered orientation, which reduces the trap state in the perovskite film and leads to suppressed recombination. The plastic PSCs based on our BPQDs ESL achieved an efficient power conversion efficiency (PCE) of 11.26%, while the PCE is 14.6% for the FTO/glass based rigid device. These results are promising when compared with the other ESL materials for PSCs at their early attempts (Table S1). This work demonstrates that the elemental material, BP, is a promising replacement to the existing ESL materials, such as metal oxides and organic molecules, for solar cells.

## 2. Experimental Section

### 2.1. Materials

BP crystals are from Smart Elements GmbH, Austria. Formamidinium iodide (H<sub>2</sub>N=CHNH<sub>2</sub>I; FAI), methylammonium iodide (CH<sub>3</sub>NH<sub>3</sub>I; MAI), methylammonium bromide (CH<sub>3</sub>NH<sub>3</sub>Br;

MABr),  $\text{PbI}_2$  and  $\text{PbBr}_2$  are purchased from Dyesol. *N,N*-dimethylformamide (DMF, 99.9%), Dimethyl Sulphoxide (DMSO, 99.9%), 4-*tert*-butylpyridine (4-TBP, 96%), lithium bistrifluoromethane sulfonimide (LiTFSI, 99.9%), chlorobenzene (99.5%) are obtained from Sigma-Aldrich. All chemicals are used as received without further purification.

### 2.2. Preparation of BPQDs

The BP crystals were ground into powder and added into NMP solution. Then the mixtures were ultrasonicated using an ultrasonic bath (400W) at 20 °C for 8 hrs. The obtained BP mixture was purified by centrifugation, with a rate of 5000 rpm for 30 min, to remove larger particles. Then the residual BP dispersion was further turned into BPQDs by probe sonication for 4 hrs.

### 2.3. Preparation of BPQDs film and PSCs

Prior to film deposition, the ITO/PEN substrate (Pecell) was etched into designed pattern by Zn powder and 2 M HCl solution and then well cleaned by the detergent, absolute ethanol and DI water successively. A subsequent 10 min  $\text{O}_2$  plasma treatment was conducted to increase wettability of the ITO surface. BPQDs films were fabricated by spin-coating the freshly prepared BPQDs IPA solution at 1500 rpm for 30 s in a  $\text{N}_2$  filled glove box. The thickness of BPQDs films were controlled by repeating the spin-coating process for different times (*i.e.* 0, 1, 3, 5, and 7). Between each coating, the as-prepared film was dry at 60 °C for 5 min. The  $\text{FA}_{0.85}\text{MA}_{0.15}\text{PbI}_{2.5}\text{Br}_{0.5}$  perovskite films were deposited on the newly coated BPQDs film with a procedure according to the reported work.<sup>43</sup> The as-deposited films were heated at 100 °C for 60 min for crystallization. For comparison purpose, perovskite films were also deposited on the bare ITO/PEN or compact  $\text{TiO}_2$  coated FTO/glass substrates under the same conditions. The high-temperature sintered  $\text{TiO}_2$  compact layer was deposited according to our

previous work.<sup>44</sup> A hole-transporting material (HTM) solution comprised of 61 mM spiro-OMeTAD, 55 mM tert-butylpyridine (TBP) and 26 mM Li-TFSI salt in chlorobenzene was spin-coated on the perovskite layer at 4000 rpm for 30 s. Au films with thickness of 80 nm were thermal-evaporated on the electrodes, which have been stored in a desiccator overnight, as the top electrode. The active area of each PSCs is  $0.09 \text{ cm}^{-2}$ .

#### 2.4. Characterization

The morphology and structure of BPQDs were characterized by the scanning transmission electron microscope (STEM, JEOL JEM-2100F) operated at 200 kV. The morphologies of both BPQDs on Si plate and BPQDs films on ITO/PEN were imaged by AFM (Veeco Dimension-Icon system) with a scanning ratio of 0.977 Hz. The micrographs of the BPQDs and perovskite films were obtained using a field-emission scanning electron microscope (FESEM, ZEISS Merlin) operated at 5 kV. The optical absorption of BPQD were studied by a UV-Vis spectrophotometer (Hitachi U-3010, Japan). Raman spectra were collected using a Horiba Jobin Yvon HR800 Raman microscopic system equipped with a 488 nm laser operating at 180 mW. The spot size of excitation laser is  $\sim 1 \mu\text{m}$ . The PL measurements were conducted on a FLS920P Edinburgh Analytical Instrument apparatus with a 485 nm laser excitation source. Photocurrent density-voltage ( $J$ - $V$ ) curves were recorded using a Keithley 2400 source meter under one sun AM 1.5 G illumination ( $100 \text{ mW cm}^{-2}$ ) supplied by a solar simulator (Enlitech SS-F7-3A, 300W). The light intensity was calibrated by a silicon reference cell (NREL) equipped with a power meter. The incident photon-to-electron conversion efficiency (IPCE) were tested by an IPCE system (Enlitech QE-R).

### 3. Results and Discussion

### 3.1. Morphological and Optical Properties of Black Phosphorus Quantum Dots

The crafted BPQDs were synthesized from the BP crystals by liquid-phase exfoliation through employing a combination of bath sonication and probe sonication in N-methyl-2-pyrrolidone (NMP). Fig. 1a shows the schematic crystal structure of BP, which is composed of

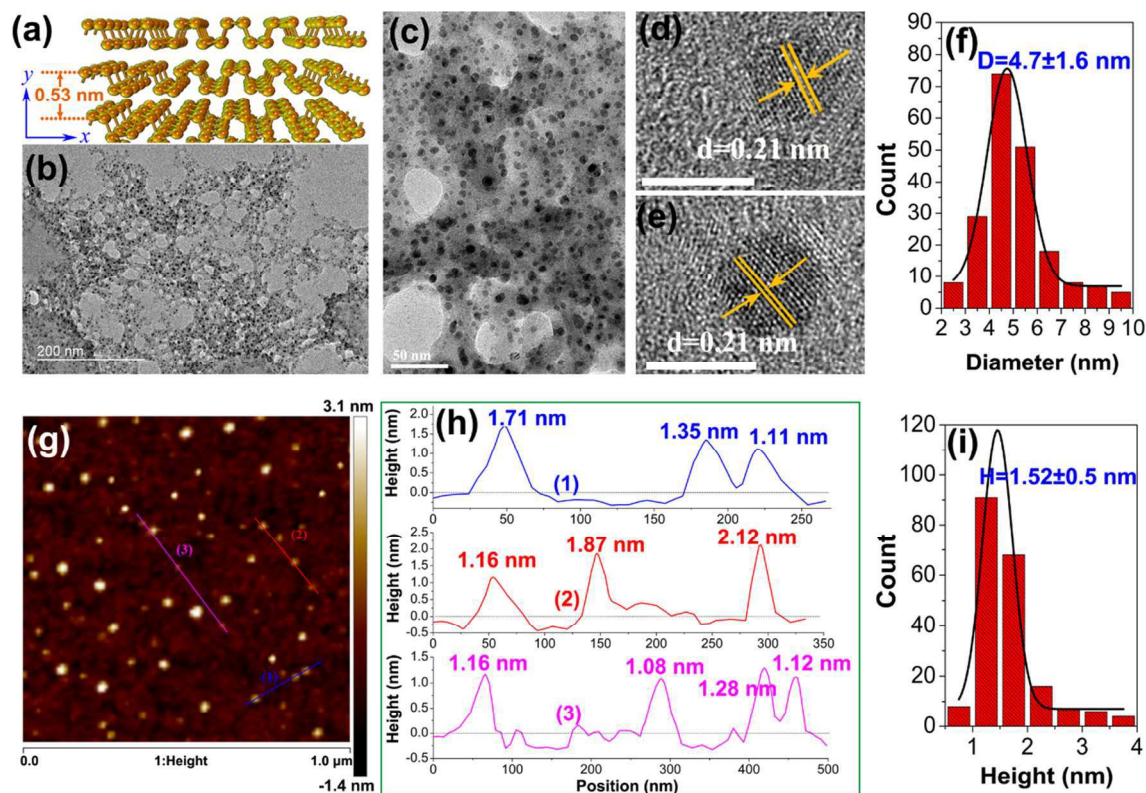


**Fig. 1** Morphology and structure characterization of black phosphorus quantum dots (BPQDs). a) Schematic diagram of layered crystal structure of bulk black phosphorus (BP); b) TEM image of the BPQDs; c) enlarged TEM image of BPQDs; d,e) High-resolution TEM image showing the lattice fringe of BPQD. Scale bar=5 nm; f) Statistical distribution of the sizes of 200 BPQDs measured from TEM images; g) AFM images of BPQDs on Si sheet; h) Height profiles along the lines marked in (g); i) Statistical distribution of the thickness of 200 BPQDs measured by AFM.

layered orthorhombic structure with the space group of  $Cmca$  (no. 64). Each P atom bonds with three others and the thickness of each layer, along y direction, is around 5.3 Å.<sup>28,29</sup>

Scanning transmission electron microscopy (STEM) and atomic force microscopy (AFM)

were employed to explore the fine microstructural morphology of the as-prepared BPQDs. The STEM images shown in Fig. 1b and 1c depict the well-dispersed BPQDs with diameters ranging from 3 nm to 10 nm. The average crystallite size of BPQDs is found to be  $4.7 \pm 1.6$  nm (Fig. 1f). The atomic structure of individual BPQDs is further analyzed by high-resolution TEM (HRTEM). The interplanar spacing of the studied BPQDs is  $\approx 0.21$  nm (Fig. 1d,e), which can be assigned to (002) crystal plane of orthorhombic phosphorus (ICDD-PDF: No. 76–1963). The AFM images showing the topographic morphology of BPQDs are displayed in Fig. 1g. The statistical average thickness of BPQDs is  $1.52 \pm 0.5$  nm (Fig. 1i), corresponding to a stack of  $3 \pm 1$  layers of BPs.

The optical properties of the obtained BPQDs were characterized by the UV/Vis absorption spectroscopy, Raman spectroscopy and ultraviolet photoelectron spectrometer (UPS). The Raman spectra of as-prepared BPQDs and bulk BP are shown in Fig. 2a. Three feature peaks can be ascribed to one out-of-plane phonon mode of  $A^1_g$  located at  $360.8 \text{ cm}^{-1}$ , and two in-plane modes of  $B_{2g}$  and  $A^2_g$  located at  $438.6$  and  $466.1 \text{ cm}^{-1}$ , respectively.<sup>25,45</sup> Compared to the bulk BP, the  $A^1_g$ ,  $B_{2g}$  and  $A^2_g$  modes of BPQDs show red-shift phenomenon.<sup>25</sup> This red-shift phenomenon is similar to the model change of graphene quantum dots,<sup>46</sup> indicating the formation of small BP fragments with thin thickness and small lateral dimensions.<sup>25</sup> The prepared BPQDs can be easily dispersed in 2-propanol as a clear yellow liquid (inset of Fig. 2b). The absorption curve of the prepared solution is illustrated in Fig. 2b. To gain the exact bandgap energy,  $E_g$ , value of the obtained BPQDs, the Tauc plot was evolved from the UV-Vis spectrum (see details in Supporting Information). According to the Tauc plot (Fig. 2c), the bandgap of BPQDs is deduced to be 1.9 eV, which is in line with the value determined from the photoluminescence (PL) spectrometry of BPQDs in isopropanol (Fig. S1) and consistent with the reported values of BPQDs with similar size.<sup>40,41</sup>

The valence band (VB) was evaluated by the VB spectrum from the UPS measurements. For the UPS test, BPQDs were coated on the ITO/PEN substrate five times to form a dense film. As shown in Fig. 2d, the VB of BPQDs on ITO substrate is tested to be  $\sim 5.74$  eV. According to the above analysis, therefore, the conduction band (CB) and VB are 3.84 and 5.74 eV, respectively.

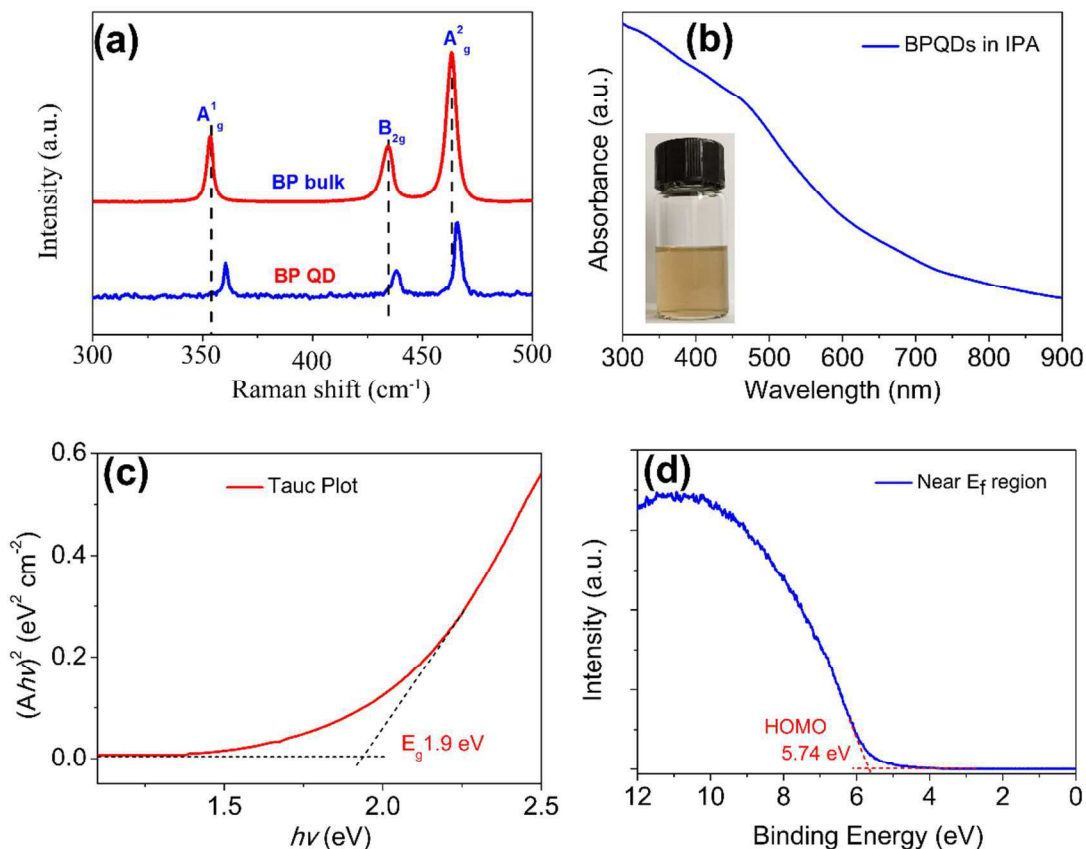


**Fig. 2** Optical characterization of black phosphorus quantum dots (BPQDs). a) Raman spectra of BPQDs and bulk crystalline BP; b) UV/Vis absorption spectrum of BPQDs in IPA. Inset is the digital photo of the BPQDs suspension with high concentration; c) Tauc plot for the corresponding absorption spectrum presented in (b); d) UPS spectrum showing the valence band of BPQDs.

### 3.2. Photovoltaic Performance of Perovskite Solar Cells

The electron and hole transport behaviors of the obtained BPQDs were investigated by measuring the performance of the BPQDs based field effect transistor (FET). The transfer

characteristics of the FET are measured at room temperature using the configuration presented as insert in Fig. S2a (More experimental details for FET test can be found in Supporting Information). Fig. S2 shows the transfer characteristics and  $I$ - $V$  curve of the BPQDs FET. The source-drain  $V_{DS}$  was set at 0.1 V while the backgate voltage  $V_G$  was varied from -20 V to 50 V. The ‘On/Off’ ratio of  $\sim 1.38$  in drain current was observed. It can be found from the transfer characteristics that the studied BPQDs FET also reveals a clearly ambipolar conductivity, as indicated in BP flakes.<sup>47</sup> The electron and hole mobility of BPQDs were estimated to be around  $1.48 \times 10^{-2}$  and  $7.8 \times 10^{-3} \text{ cm}^2 \text{ V}^{-1} \text{ s}^{-1}$ , respectively. Since the BPQDs demonstrate fascinating advantages of ambipolar conductivity for both electron and hole as well as sizable bandgap, it motivates us to exploit BPQDs as SEL for plastic PSCs, with the device architecture shown in Fig. 3a. Firstly, we assessed the possibility of BPQDs as ESL for PSCs, from the energy level (*i.e.* conduction and valence band) point of view. The band alignment of the structured PSCs is sketched in Fig. 3b, which reveals that both CB and VB levels of the BPQDs films match well with that of  $\text{FA}_{0.85}\text{MA}_{0.15}\text{PbI}_{2.5}\text{Br}_{0.5}$  perovskite (3.8 and 5.4 eV for CB and VB, respectively) to form a cascade energy level, facilitating the electron transfer but rejecting the hole extraction from the absorber to the BPQDs ESL.

The microstructure of the PSCs was imaged by the scanning electron microscopy. The cross-section SEM image of the PSCs device displayed in Fig. 3c showcases a well-defined layered structure with sharp interfaces. The thicknesses of BPQDs ESL (5 layers), perovskite, Spiro-OMeTAD, and Au are around 30, 500, 160, and 80 nm, respectively. To uncover the effects of ESL thickness on the device performance, BPQDs films with various thicknesses (*i.e.* 0, 1, 3, 5, 7 layers) were deposited by controlling the spin-coating times of BPQDs solution. The current density-voltage ( $J$ - $V$ ) curves of the plastic PSCs with and without BPQDs ESL are shown in Fig. 3d and Fig. S3. The detailed photovoltaic parameters of

devices with BPQDs layers of different thickness are summarized in Table 1. For the PSCs without any ESL, i.e. the perovskite layer deposited directly on bare ITO, the device yields a low PCE of 3.58%. With the increase of BPQDs thickness, all photovoltaic parameters gain a simultaneous improvement (Table 1). The PSCs built on the ESL with five layers of BPQDs exhibits a much higher short-circuit current density ( $J_{sc}$ ) of  $16.77 \text{ mA cm}^{-2}$ , an open-circuit photovoltage ( $V_{oc}$ ) of 1.03 V, and

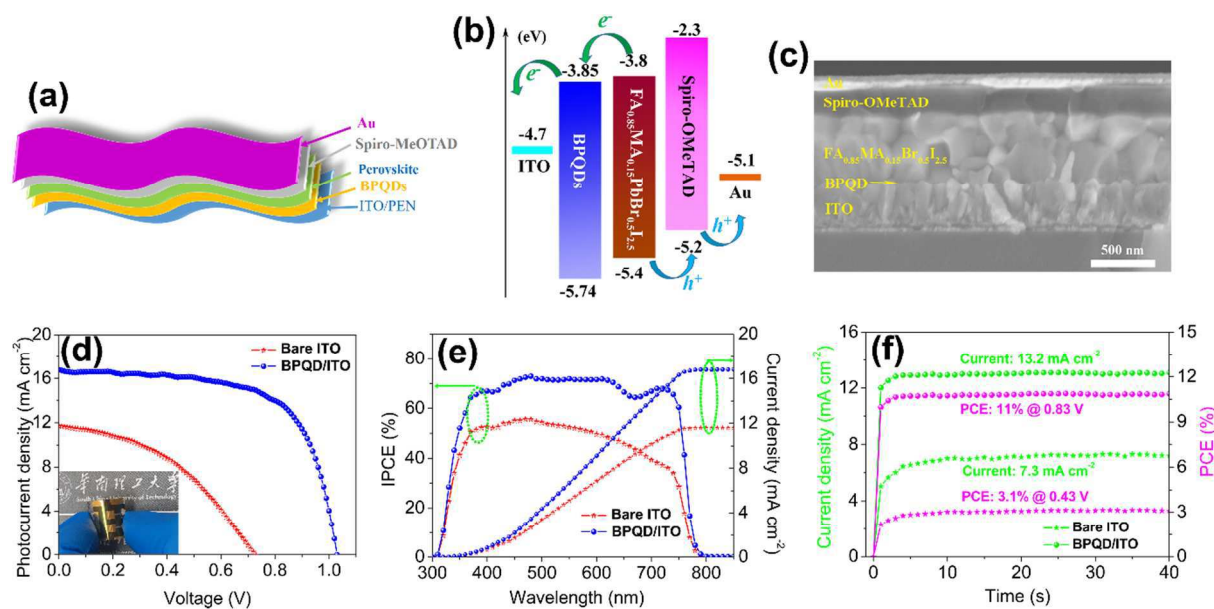


**Fig. 3** a) Schematic illustration of the plastic organic-inorganic perovskite solar cells in this work; b) Energy level diagram of each component of PSCs. c) Cross-sectional SEM image showing the functional layers of the PSCs; d)  $J$ - $V$  characteristic curves of PSCs built on BPQDs electron selective layer (ESL) and bare ITO substrate, measured under 1 sun illumination ( $100 \text{ mW cm}^{-2}$ ) in a reverse scan. The inset is the digital image of the plastic PSC; e) IPCE spectra and integrated  $J_{sc}$  curves of PSCs built on BPQDs ESL and bare ITO substrate; f) Stabilized power output of the devices constructed on BPQDs ESL and bare ITO, measured by keeping the cells at a fixed voltage near the maximum power point on the  $J$ - $V$  curves.

**Table 1** Photovoltaic parameters of the PSCs constructed on the ITO/PEN substrate with BPQDs layers of different thickness as electron selective layer.

Device	$J_{sc}$	$V_{oc}$	$FF$	PCE	$R_s$	$R_{sh}$
--------	----------	----------	------	-----	-------	----------

	[mA cm <sup>-2</sup> ]	[V]		[%]		
Bare ITO	11.71	0.728	0.421	3.58	369	4070
BPQD-1	14.69	0.894	0.483	6.46	214	7737
BPQD-3	15.98	0.945	0.581	8.77	166	18750
BPQD-5	16.77	1.03	0.652	11.26	58	29948
BPQD-7	15.76	0.897	0.552	7.81	362	4055

a fill factor (*FF*) of 0.652, achieving a PCE up to 11.26% which is more than three times the efficiency of the device without an electron selective materials.

The incident photon-to-electron conversion efficiency (IPCE) measurements were conducted to demonstrate the significant improvement of the device performance. As depicted in Fig. 3e, the device without ESL exhibits a relative low IPCE. In contrast, remarkably higher IPCE values were obtained in the device employed BPQDs (5 layers) as ESL over the entire measuring wavelength range of 300-800 nm. The  $J_{sc}$  integrated from the IPCE results are 11.28 and 16.37 mA cm<sup>-2</sup> for the PSCs without and with BPQDs ESL, respectively, which are in good agreement with those obtained from the *J-V* tests. To assess the reliability of the extracted  $J_{sc}$  and PCE from the *J-V* curves, we examined the stabilized power output (SPO), in terms of photocurrent density as a function of time, by recording the photocurrent over a bias at the fixed maximum power point for 40 s. As illustrated in Fig. 3f, the device constructed on the bare ITO/PEN substrate shows a stabilized photocurrent of around 7.3 mA cm<sup>-2</sup> and a stable PCE of about 3.1%, corresponding to a relatively low SPO-to-PCE ratio (SPO ratio) of 88%. In contrast, the PSC built on the BPQDs ESL (5 layers) yields a steady photocurrent of about 13.2 mA cm<sup>-2</sup> and a PCE of around 11%, respectively, resulting in a substantially improved SPO ratio of 97.7%. The higher SPO ratio of BPQDs based PSCs

might stem from the more efficient extraction and transport of photo-generated electrons from absorber to collective electrode by BPQDs ESL. Additionally, we also study the performance of low-temperature produced BPQDs ESL for rigid PSCs built on FTO/glass substrate. The rigid PSCs with BPQDs ESL yields a much higher  $J_{sc}$  of 18.49 mA cm<sup>-2</sup> and a PCE of 14.6% (Fig. S4), which is not much far behind that of a rigid PSC based on an annealed (450 °C) TiO<sub>2</sub> compacted electron transport layer (17.9%, Fig. S5).

In order to improve the PCE of a PSC, a compact ESL is essential to extract the photo-generated electrons but impede the transfer of hole from the excited perovskite absorber to the collective electrode, inhibiting the direct carrier recombination (radiative recombination) at the ITO interface. The morphology of ESL films with BPQDs of various thickness were observed by SEM and AFM. As revealed by the SEM images (Fig. S6a-c), the bare ITO surface with accidented grain is covered gradually by BPQDs as the coating times increased. A smooth and dense surface without obvious BPQDs aggregation is finally achieved when five layers of BPQDs with a thickness around 30 nm were deposited. However, further increase of the number of layers, e.g. 7 layers, leads to severe aggregation of the BPQDs (Fig. S6d). The 3D AFM images shown in Fig. S7 reveal that the root-mean-square roughness ( $R_q$ ) of BPQDs coated electrode decreases from 4.2 nm of bare ITO to 1.86 nm upon the increase of coating times from 0 to 5, indicating the formation of smooth BPQDs films. In our case, the formation of dense BPQDs films (5 layers) on the ITO surface provides an efficient electron transport pathway (low total series resistance,  $R_s$ , Table 1), thus significantly reducing direct charge recombination and leading to the remarkable enhancement in  $FF$  and  $V_{oc}$ . The suppressed charge recombination also results in reduced charge loss and boosts the  $J_{sc}$  and PCE.

### 3.3. Morphological and Structural Quality of the Perovskite Films

It is reported that the trap-assisted non-radiative charge recombination plays a dominant role in the efficiency loss in PSCs.<sup>3,48,49</sup> The existence of the traps is strongly correlated with the disorder of the grains caused by ionized impurities, lattice vacancies and grain-boundary defects within perovskite films.<sup>49,50</sup> Therefore, control over morphology and crystallinity of perovskite film is of decisive importance to achieve high-performance PSCs.<sup>3,51</sup> Fig. 4 shows the typical SEM images of the perovskite films deposited on the bare ITO surface and BPQDs

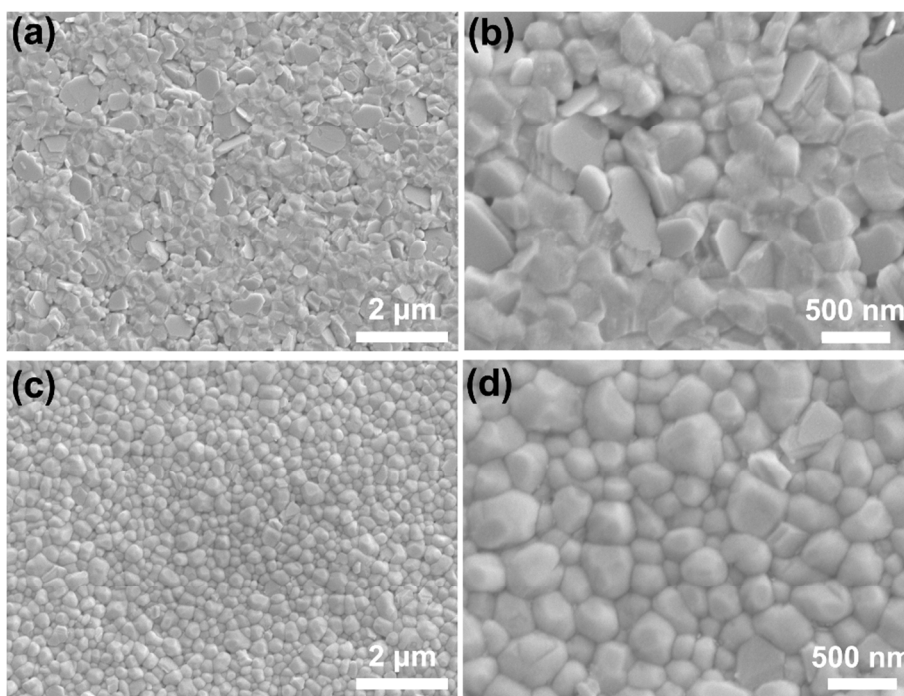


**Fig. 4** Perovskite film quality characterization: a) low-magnification and b) high-magnification SEM image of perovskite film deposited on bare ITO/PEN substrate; c) low-magnification and d) high-magnification SEM image of perovskite film deposited on BPQDs coated ITO/PEN substrate.

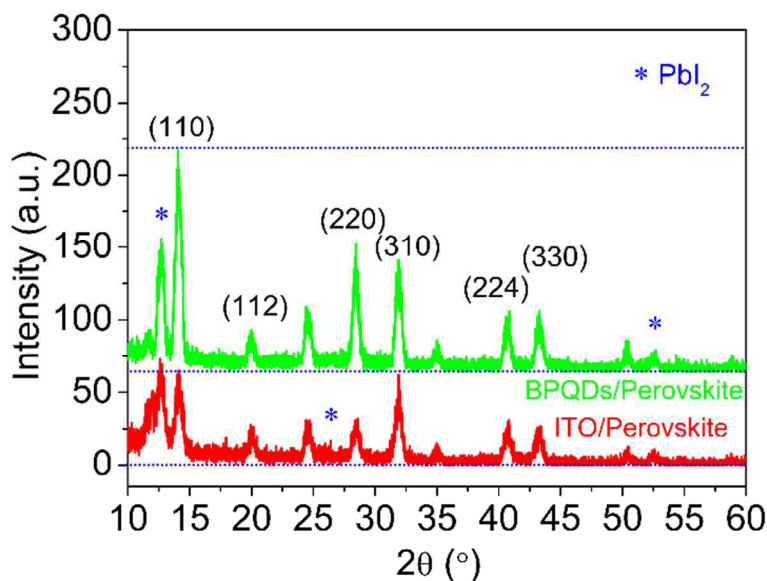


**Fig. 5** XRD patterns of FA<sub>0.85</sub>MA<sub>0.15</sub>PbI<sub>2.5</sub>Br<sub>0.5</sub> perovskite deposited on bare ITO/PEN substrate and on BPQDs coated ITO/PEN electrode.

film coated ITO surface. As depicted in Fig. 4a,b, the perovskite film deposited on the bare ITO surface shows a random stacking of perovskite nanoplates surrounded by some phase with indefinite appearances, exhibiting an obscure grain boundaries. The X-Ray diffraction (XRD) pattern (Fig. 5) of the perovskite film deposited on bare ITO reveals the existence of large amount of PbI<sub>2</sub>, which may be the phase surrounding the perovskite grains. Herz's work confirmed that the trap-assisted recombination could be greatly accelerated, due to the presence of composition inhomogeneity in this disordered region.<sup>49,50</sup> According to the XRD patterns, one can easily get that the perovskite film growth on the BPQDs ESL contains around 2 times less PbI<sub>2</sub>, compared with the one deposited on bare ITO surface. Usually, a moderate residual of PbI<sub>2</sub> can deliver stable and high efficiency of PSCs, while too much PbI<sub>2</sub> resided in the active film leads to poor transit stability and deteriorates cell performance.<sup>52</sup> Moreover, there are also numbers of voids and pinholes in the perovskite film deposited on the bare ITO surface, which will create severe shorting sites for direct charge recombination and lead to a significant efficiency loss as well.<sup>50</sup> For the FA<sub>0.85</sub>MA<sub>0.15</sub>PbI<sub>2.5</sub>Br<sub>0.5</sub> film coated

on the BPQDs ESL, the grains with a size of 100-500 nm were densely packed without observable pinholes and voids (Fig. 4c,d). The low-magnification SEM image shown in Fig. 4c further demonstrates a uniform and regular morphology with well-defined grain boundary. The cross-sectional (Fig. 3c) and top viewed SEM (Fig. 4d) also reveals that the grains are packed with ordered orientation and well-defined grain boundaries, suggesting the good crystallinity. A comparison of the SEM images of the perovskite deposited on bare ITO, BPQDs coated ITO (Fig. 4), and low-temperature produced TiO<sub>2</sub> coated ITO (Fig. S8) suggests that the BPQDs ESL will facilitate the formation of perovskite grains with compact stacking, order orientation and less surface roughness. We speculate that the obtained BPQDs with excellent crystallinity (shown in Fig. 1d,e) may act as crystal nuclei for the growth of ultrafine perovskite grains. It is well known that the crystallinity of perovskite active domains will greatly affect the charge dissociation, transport, and diffusion length and thus determines the final performance of the solar cells.<sup>53</sup> The XRD patterns shown in Fig 5 confirm an increased crystallinity of the BPQDs/perovskite as almost all of the diffraction peaks, especially the (110) and (220), show a remarkably increased peak intensity when compared to the bare-ITO/perovskite sample, given that the thickness and the test condition for the both films are identical. The strong reflection at 14.2° and 28.5° can be assigned to the (110) and (220) crystal planes of the mixed halide perovskite.<sup>50-53</sup> As compared to other crystal planes, the intensity of (110) and (220) peaks of BPQDs/perovskite are significant stronger, indicating the texture with the (110) crystal plane preferentially oriented parallel to the film surface,<sup>53</sup> which is in consistent with the observation in SEM measurements. In contrast, no preferential orientation can be observed from both the XRD and SEM tests for the ITO/perovskite film. Therefore, the high-quality perovskite film derived from BPQDs film is

also responsible for the great improvement in device performance, besides the fast electron extraction mentioned above.

### 3.4 Optoelectronic Performance of the Perovskite Electrodes

To gain further insights into the effects of BPQDs ESL on the perovskite film quality and charge extraction behavior, the optoelectronic properties of the perovskite film were examined by steady-state photoluminescence (PL) spectrometry and time-resolved PL decay (TRPL). As depicted in Fig. 6, the steady-state PL intensity of perovskite film deposited on BPQDs ESL (BPQDs/Perovskite) is about four folds lower than that of perovskite film on bare ITO substrate, indicating the excellent electron extraction from absorber by the BPQDs. Meanwhile, the steady-state PL peak locates at 762 nm for the BPQDs/Perovskite, which shows smaller Stokes shift compared to that of ITO/Perovskite (at 768 nm), demonstrating the milder vibronic relaxation and reduced crystallization defects of the perovskite film on BPQDs ESL.<sup>51,54</sup> The charge carries lifetime was characterized by the TRPL to further explore the nature for the significantly improved efficiency of BPQDs ESL based PSCs. The TRPL decays of both BPQDs/Perovskite and bare ITO/Perovskite exhibit a bi-exponential decay feature containing a fast decay and a slow decay components, as shown in Fig. 6b and Table S2. It is believed that the fast decay is related to the bimolecular recombination of free charge carriers (electron-hole here) in terms of a direct band-to-band recombination (radiative recombination), while slow decay is arisen from the monomolecular charge-recombination which is predominantly originated from trapping of charges (non-radiative recombination).<sup>48,49,55</sup> The fast decay is considered to be the result of quenching the free charges during the charge transport in the perovskite domains and then the transfer into ESL. For the ITO/Perovskite film, the fast decay lifetime ( $\tau_1$ ) and slow decay lifetime ( $\tau_2$ ) are 6.8

and 198.2 ns, respectively. The average lifetime ( $\tau_{\text{ave}}$ ) was calculated to be 184.6 ns, according to Equation 1.<sup>56</sup> In contrast, the BPQDs/Perovskite film exhibits a significant decrease of  $\tau_1$ ,  $\tau_2$  (4.3 ns and 27.6 ns, respectively). The  $\tau_{\text{ave}}$  (18.3 ns) are one order of magnitude lower than that of the ITO/Perovskite sample, indicating the fast transfer of photo-generated electrons from the absorber to the conductive electrode.

$$\tau_{\text{ave}} = \frac{\sum_{i=1}^n \frac{A_i \tau_i^2}{A_i \tau_i}}{\frac{A_1 \tau_1 + A_2 \tau_2}{A_1 \tau_1 + A_2 \tau_2}} \quad (\text{Equation 1})$$

$$c_i = \frac{A_i}{\sum_{i=1}^n A_i} \quad (\text{Equation 2})$$

where,  $A_i$ ,  $\tau_i$ ,  $c_i$  are pre-exponential factors, lifetime and weight concentration for each decay component, respectively.  $\tau_{\text{ave}}$  is the average lifetime of entire decay process. Here,  $n=2$ ,  $i=1, 2$ . The fast electron transfer will result in suppressed radiative recombination, owing to the well aligned band level, high charge mobility of dense BPQDs film, and the obtained high-quality perovskite films as well.<sup>48,49,53</sup> According to Equation 2,<sup>56</sup> the weight concentration ( $c$ ) for the fast decay component ( $c_1$ ) is 71.1% in the ITO/Perovskite sample and 80.3% in the BPQDs/Perovskite. The decreased lifetime and increased weight fraction of the fast decay process ( $\tau_1$  and  $c_1$ ) of BPQDs/Perovskite device suggest that most of the photoelectrons generated in the perovskite film are efficiently transferred into the BPQDs ESL, due to the good electron extracting capacity of BPQDs and the formation of high-quality perovskite film. The reduction of the trap-states and trap-assisted recombination of BPQDs ESL based PSCs can also be confirmed from the photovoltaic characterization. As indicated by the stabilized power output tests (Fig. 3f), the PSCs based on the BPQDs/Perovskite takes up less than 5 s to get a stabilized efficiency output whereas  $\sim 15$  s is required to achieve a stable

power output for the device built on the bare ITO, indicating the less defects that need to be filled up in the PBQDs/Perovskite film. Therefore, we can conclude that the dual functional BPQDs can act as ESL for fast electron extraction from perovskite absorber and an excellent template for growth of fine perovskite films. The high-quality perovskite film formed on the BPQD ESL suppresses both the radiative and non-radiative recombination, thus reducing charge loss. Consequently, a high efficiency is achieved in the BPQDs based plastic PSCs.

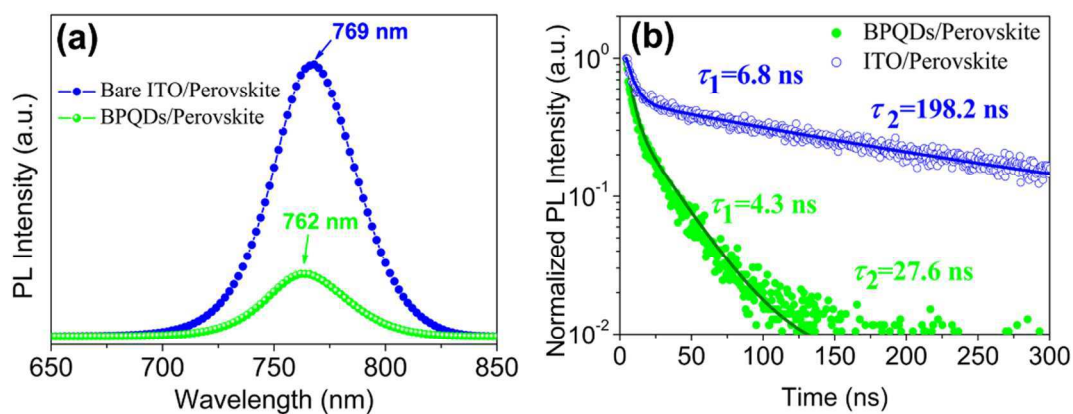


**Fig. 6** Perovskite film quality characterization: a) Steady state photoluminescence (PL) and b) Time-resolved photoluminescence (TRPL) decay trace of the perovskite film deposited on BPQDs/ITO/PNE and bare ITO/PEN substrate.

### 3.5 Bending Test of the Plastic Solar Cells

Flexibility is a desirable feature of the plastic solar cells. To assess the flexibility of the BPQDs based plastic, the obtained device was repeatedly bend with a radius of around 5 mm, with a frequency of 1 Hz. The photovoltaic parameters variations as a function of bending cycles are shown in Fig. S9. It clear that there are no significant changes of  $J_{sc}$  and  $V_{oc}$ , as the bending cycle increased. The SEM images shown in Fig. S10 observed no cracks of perovskite films after 200 cycles of bending, indicating that the active layer and even each interfaces between the functional layers are not damages by the shape wrench. However, the  $FF$  declined remarkably from 0.657 to 0.583, leading to a reduction of PCE from 11.32 to

10.04%, with about 88.7% of the initial PCE being retained. The increased sheet resistance of the ITO/PEN substrate is likely to be the predominant reason for the deterioration of  $FF$  and PCE, since the drastic bending can cause crack formation for the rigid ITO conductive film.<sup>57</sup>

#### 4. Conclusions

In summary, we reported the exploitation of solution processed BPQDs as a novel and dual-functional electron selective layer for efficient plastic planar-heterojunction PSCs. The formation of well-aligned band cascade between the perovskite absorber and ITO charge collector by the fine BPQDs facilitates the efficient charge extraction and transport. The BPQDs can also facilitate the gain of dense perovskite films with enhanced crystallization. This high-quality perovskite films are pinhole-free and of significantly decreased trap-state, which consequently suppresses radiative recombination and trap-assisted non-radiative recombination in the photovoltaic devices. The low-temperature produced plastic PSCs employing this newly developed electron transport material yield a promising power conversion efficiency up to 11.26%. We believe that further improvement in efficiency can be achieved through chemical modification of BPQDs.

#### Acknowledgments

This work is financially supported by the National Natural Science Foundation of China (Grants No. 61604058), the Fundamental Research Funds for the Central Universities (2017MS003). This work is also supported by the Science and Technology Research Items of Shenzhen (No.JCYJ20160422102802301 and KQJSCX2016022619562452), the Hong Kong, Macao and Taiwan Science & Technology Cooperation Program of China (No.2015DFH10200), the project (G1602) of Guangdong Research Center for Interfacial

Engineering of Functional Materials, College of Materials Science and Engineering, Shenzhen University, and Australian Research Council Discovery Project (DP170103514).

### Electronic supplementary information (ESI)

Electronic supplementary information (ESI) available:

### Reference

- 1 A. Kojima, K. Teshima, Y. Shirai, T. Miyasaka and *J. Am. Chem. Soc.*, 2009, **131**, 6050-6051.
- 2 W. S. Yang, B. W. Park, E. H. Jung, N. J. Jeon, Y. C. Kim, D. U. Lee, S. S. Shin, J. Seo, E. K. Kim, J. H. Noh and S. Il. Seok, *Science*, 2017, **356**, 1376-1379.
- 3 M. He, B. Li, X. Cui, B. B. Jiang, Y. J. He, Y. H. Chen, D. O'Neil, P. Szymanski, M. A. El-Sayed, J. S. Huang and Z. Q. Lin, *Nat. Commun.*, 2017, **8**, 16045.
- 4 J. H. Heo, H. J. Han, D. Kim, T. K. Ahn and S. H. Im, *Energy Environ. Sci.*, 2015, **8**, 1602-1608.
- 5 W. Li, W. Zhang, S. V. Reenen, R. J. Sutton, J. Fan, A. A. Haghighirad, M. B. Johnston, L. Wang and H. J. Snaith, *Energy Environ. Sci.*, 2016, **9**, 490-498.
- 6 T. Leijtens, G. E. Eperon, S. Pathak, A. Abate, M. M. Lee and H. J. Snaith, *Nat. Commun.*, 2013, **4**, 2885.
- 7 D. Yang, R. X. Yang, J. Zhang, Z. Yang, S. Z. (Frank) Liu and C. Li, *Energy Environ. Sci.*, 2015, **8**, 3208-3214.
- 8 N. Q. Fu, Y. Y. Fang, Y. D. Duan, X. W. Zhou, X. R. Xiao and Y. Lin, *ACS Nano*, 2012, **6**, 9596-9605.

- 9 M. Kaltenbrunner, G. Adam, E. D. Głowacki, M. Drack, R. Schwödiauer, L. Leonat, D. H. Apaydin, H. Groiss, M. C. Scharber, M. S. White, N. S. Sariciftci and S. Bauer, *Nat. Mater.*, 2015, **14**, 1032-1039.
- 10 J. You, Z. Hong, Y. (Michael) Yang, Q. Chen, M. Cai, T. B. Song, C. C. Chen, S. Lu, Y. Liu, H. Zhou and Y. Yang, *ACS Nano*, 2014, **8**, 1674-1680.
- 11 C. Bi, B. Chen, H. Wei, S. D. Luca and J. Huang, *Adv. Mater.* 2017, **29**, 1605900.
- 12 Z. Zhu, J. Q. Xu, C. C. Chue, H. Liu, Z. Li, X. Li, H. Chen and A. K.-Y. Jen, *Adv. Mater.*, 2016, **28**, 10786-10793.
- 13 D. Yang, R. Yang, X. Ren, X. Zhu, Z. Yang, C. Li and S. (Frank) Liu, *Adv. Mater.*, 2016, **28**, 5206-5213.
- 14 J. M. Ball, M. M. Lee, A. Hey and H. J. Snaith, *Energy Environ. Sci.*, 2013, **6**, 1739-1743.
- 15 J. H. Heo, M. H. Lee, H. J. Han, B. R. Patil, J. S. Yub and S. H. Im, *J. Mater. Chem. A*, 2016, **4**, 1572-1578.
- 16 Q. Jiang, L. Zhang, H. Wang, X. Yang, J. Meng, H. Liu, Z. Yin, J. Wu, X. Zhang and J. You, *Nat. Energy*, 2016, **14**, 16177.
- 17 M. Park, J.-Y. Kim, H. J. Son, C.-H. Lee, S. Soon Jang, M. J. Ko, *Nano Energy*, 2016, **26**, 208-215.
- 18 S. S. Shin, W. S. Yang, J. H. Noh, J. H. Suk, N. J. Jeon, J. H. Park, J. S. Kim, W. M. Seong and S. Il Seok, *Nat. Commun.*, 2015, **6**, 7410.
- 19 Y. Hou, C. O. R. Quiroz, S. Scheiner, W. Chen, T. Stubhan, A. Hirsch, M. Halik, and C. J. Brabec, *Adv. Energy Mater.*, 2015, **5**, 1501056.

- 20 P. Chen, X. Yin, M. Que, X. Liu and W. Que, *J. Mater. Chem. A*, 2017, **5**, 9641-9648.
- 21 J. Feng, Z. Yanga, D. Yang, X. Ren, X. Zhu, Z. Jin, W. Zi, Q. Wei, S. (Frank) Liu, *Nano Energy*, 2017, **36**, 1-8.
- 22 V. Nicolosi, M. Chhowalla, M. G. Kanatzidis, M. S. Strano and J. N. Coleman, *Science*, 2013, **340**, 1226419.
- 23 M. Chhowalla, H. S. Shin, G. Eda, L. J. Li, K. P. Loh and H. Zhang, *Nat. Chem.*, 2013, **5**, 263-275.
- 24 H. Liu, Y. C. Du, Y. X. Deng and P. D. Ye, *Chem. Soc. Rev.*, 2015, **44**, 2732-2743.
- 25 X. Zhang, H. M. Xie, Z. D. Liu, C. L. Tan, Z. M. Luo, H. Li, J. D. Lin, L. Sun, W. Chen, Z. C. Xu, L. H. Xie, W. Huang and H. Zhang, *Angew. Chem. Int. Ed.*, 2015, **54**, 3653-3657.
- 26 M. S. Zhu, Y. Osakada, S. Kim, M. Fujitsuka and T. Majima, *Appl. Catal. B: Environ.*, 2017, **217**, 285-292.
- 27 S. H. Lin, Y. S. Chui, Y. Y. Li and S. P. Lau, *FlatChem*, 2017, **2**, 15-37.
- 28 A. Castellanos-Gomez, *J. Phys. Chem. Lett.*, 2015, **6**, 4280-4291.
- 29 J. P. Lu, J. Yang, A. Carvalho, H. W. Liu, Y. Lu, C. H. Sow, *Acc. Chem. Res.*, 2016, **49**, 1806-1815.
- 30 R. W. Keyes, *Phys. Rev.*, 1953, **92**, 580-584.
- 31 Y. Hou, C. O. R. Quiroz, S. Scheiner, W. Chen, T. Stubhan, A. Hirsch, M. Halik and C. J. Brabec, *Adv. Energy Mater.*, 2015, **5**, 1501056.
- 32 L. Li, Y. Yu, G. J. Ye, Q. Ge, X. Ou, H. Wu, D. Feng, X. H. Chen and Y. Zhang, *Nat. Nanotechnol.*, 2014, **9**, 372-377.
- 33 X. H. Ren, Z. J. Li, Z. Y. Huang, D. Sang, H. Qiao, X. Qi, J. Li, J. X. Zhong and H. Zhang, *Adv. Funct. Mater.*, 2017, **27**, 1606834.

- 34 M. S. Zhu, S. Kim, L. Mao, M. Fujitsuka, J. Y. Zhang, X. C. Wang and T. Majima, *J. Am. Chem. Soc.*, 2017, **139**, 13234-13242.
- 35 M. S. Zhu, X. Y. Cai, M. Fujitsuka, J. Y. Zhang and T. Majima, *Angew. Chem. Int. Ed.*, 2017, **56**, 2064–2068.
- 36 T. Wang, S. Hu, B. Chamlagain, T. Hong, Z. Zhou, S. M. Weiss and Y. Q. Xu, *Adv. Mater.*, 2016, **28**, 7162-7166.
- 37 C. Hao, B. Yang, F. Wen, J. Xiang, L. Li, W. Wang, Z. Zeng, B. Xu, Z. Zhao, Z. Liu and Y. Tian, *Adv. Mater.*, 2016, **28**, 3194-3201.
- 38 J. Sun, H. W. Lee, M. Pasta, H. Yuan, G. Zheng, Y. Sun, Y. Li and Y. Cui, *Nat. Nanotechnol.*, 2015, **10**, 980-985.
- 39 Y. Yang, J. Gao, Z. Zhang, S. Xiao, H. H. Xie, Z. B. Sun, J. H. Wang, C. H. Zhou, Y. W. Wang, X. Y. Guo, P. K. Chu and X. F. Yu, *Adv. Mater.*, 2016, **28**, 8937-8944.
- 40 S. H. Liu, S. H. Lin, P. You, C. Surya, S. P. Lau and F. Yan, *Angew. Chem. Int. Ed.*, 2017, **56**, 13717.
- 41 W. Chen, K. W. Li, Y. Wang, X. Y. Feng, Z. W. Liao, Q. C. Su, X. N. Lin and Z. B. He, *J. Phys. Chem. Lett.*, 2017, **8**, 591-598.
- 42 S. H. Lin, S. H. Liu, Z. B. Yang, Y. Y. Li, T. W. Ng, Z. Q. Xu, Q. L. Bao, J. H. Hao, C. S. Lee, C. Surya, F. Yan and S. P. Lau, *Adv. Funct. Mater.*, 2016, **26**, 864-871.
- 43 T. J. Jacobsson, J. P. Correa-Baena, M. Pazoki, M. Saliba, K. Schenk, M. Grätzel and A. Hagfeldt, *Energy Environ. Sci.*, 2016, **9**, 1706-1724.
- 44 N. Q. Fu, Z. Y. Bao, Y. L. Zhang, G. G. Zhang, S. M. Ke, P. Lin, J. Y. Dai, H. T. Huang and D. Y. Lei, *Nano Energy*, 2017, **41**, 654-664.
- 45 X. Huang, Z. Y. Zeng and H. Zhang, *Chem. Soc. Rev.*, 2013, **42**, 1934-1946.
- 46 Y. Li, Y. Hu, Y. Zhao, G. Shi, L. Deng, Y. Hou and L. Qu, *Adv. Mater.*, 2011, **23**, 776-

780.

47 S. Das, M. Demarteau and A. Roelofs, *ACS Nano*, 2014, **8**, 11730-11738.

48 G. J. A. H. Wetzelaer, M. Scheepers, A. M. Sempere, C. Momblona, J. Ávila and H. J. Bolink, *Adv. Mater.*, 2015, **27**, 1837-1841.

49 M. B. Johnston and L. M. Herz, *Acc. Chem. Res.*, 2016, **49**, 146-154.

50 W. Rehman, R. L. Milot, G. E. Eperon, C. Wehrenfennig, J. L. Boland, H. J. Snaith, M. B. Johnston and L. M. Herz, *Adv. Mater.*, 2015, **27**, 7938-7944.

51 M. Z. Long, T. K. Zhang, W. Y. Xu, X. L. Zeng, F. Y. Xie, Q. Li, Z. Chen, F. Zhou, K. S. Wong, K. Y. Yan and J. B. Xu, *Adv. Energy Mater.*, 2017, **7**, 1601882.

52 T. J. Jacobsson, J.-P. Correa-Baena, E. H. Anaraki, B. Philippe, S. D. Stranks, M. E. F. Bouduban, W. Tress, K. Schenk, J. Teuscher, J.-E. Moser, H. Rensmo and A. Hagfeldt, *J. Am. Chem. Soc.*, 2016, **138**, 10331-10343.

53 P. W. Liang, C. Y. Liao, C. C. Chueh, F. Zuo, S. T. Williams, X. K. Xin, J. Lin and A. K. Y. Jen, *Adv. Mater.*, 2014, **26**, 3748-3754.

54 S. D. Stranks, G. E. Eperon, G. Grancini, C. Menelaou, M. J. Alcocer, T. Leijtens, L. M. Herz, A. Petrozza and H. J. Snaith, *Science*, 2013, **342**, 341-344.

55 X. P. Zheng, B. Chen, J. Dai, Y. J. Fang, Y. Bai, Y. Lin, H. Wei, X. C. Zeng and J. S. Huang, *Nat. Energy*, 2017, **2**, 17102.

56 B. Valeur, Principles of Steady-State and Time-Resolved Fluorometric Techniques, In *Molecular Fluorescence: Principles and Applications*, Wiley-VCH Verlag GmbH, Weinheim, FRG, 2001; pp 155-199.

57 C. Wang, L. Guan, D. Zhao, Y. Yu, C. R. Grice, Z. Song, R. A. Awni, J. Chen, J. Wang, X. Zhao and Y. Yan, *ACS Energy Lett.*, 2017, **2**, 2118-2124.

## Table of Contents

**Dual-functional black phosphorus quantum dots electron selective layer** was designed for plastic perovskite solar cells. The efficient electron extraction and significantly improved perovskite film quality contributed to the reasonably high efficiency.

